Coupled wedge waves

Bradley C. Abell and Laura J. Pyrak-Nolte[a)]
Department of Physics, Purdue University, 525 Northwestern Avenue, West Lafayette, Indiana 47907

(Received 21 June 2013; revised 28 August 2013; accepted 3 September 2013)

The interface between two wedges can be treated as a displacement discontinuity characterized by elastic stiffnesses. By representing the boundary between the two quarter-spaces as a displacement discontinuity, coupled wedge waves were determined theoretically to be dispersive and to depend on the specific stiffness of the non-welded contact between the two wedges. Laboratory experiments on isotropic and anisotropic aluminum confirmed the theoretical prediction that the velocity of coupled wedge waves, for a non-welded interface, ranged continuously from the single wedge wave velocity at low stress to the Rayleigh velocity as the load applied normal to the interface was increased. Elastic waves propagating along the coupled wedges of two quarter-spaces in non-welded contact are found to exist theoretically even when the material properties of the two quarter-spaces are the same. © *2013 Acoustical Society of America*. [http://dx.doi.org/10.1121/1.4821987]

PACS number(s): 43.35.Cg, 43.35.Pt, 43.20.Jr, 43.20.Bi [MD] Pages: 3551–3560

I. INTRODUCTION

Elastic waves, that propagate along the wedge formed by two intersecting planes with stress free boundaries, were originally studied for elastic waves propagating along crystal structures such as acoustic phonons and surface magnons[1] and as a use for delay-lines.[2] Since their discovery, many well documented theoretical[3] and experimental[4–8] studies of wedge waves (WWs) have been conducted (also see review articles[9–11]). WWs were found to exhibit characteristic properties that differ from other types of surface waves that make them useful for delay line applications. For example, the energy in these waves is highly localized and exists only within a few wavelengths of the wedge tip. WWs were also found to be extremely polarization dependent.[1,3,4] Several wedge modes can propagate below the Rayleigh velocity for small angle wedges ($<45°$), but as the wedge angle increases, higher evanescent modes exist with velocities greater than the Rayleigh velocity.[3] Theoretically, these flexural modes are dispersionless for a perfectly smooth surface and a very sharp wedge tip;[2] however, for imperfect wedges (i.e., rough edges) a dispersive waveform was both theorized and observed experimentally.[5,12]

Research on WWs expanded into areas of plate theory studies,[13] different wedge geometries,[14,15] wedge diffraction,[16] dispersion,[17] anisotropy[18,19] and electrostatic wave theory.[20,21] Experimentally WWs were studied for water loaded wedges,[22,23] laser induced waves[7,24] and wedge imperfection studies[5] for a wide range of wedge angles ($0°-120°$). No analytical expression that accurately postulates the WW velocity for wedge angles of $90°$ has been found, but numerical approximations have been determined to be in good agreement with experimental measurements.[6]

WW applications also include coupling along different geometries and boundary conditions.[25–27] More recently, the numerical approximations set forth by Maradudin *et al.*[1] were used to couple two orthogonal wedges with different isotropic properties.[28] The coupling gave rise to a new type of waveform, named Rayleigh–Stoneley (RS) waves, that propagate along the coupled tips of two isotropic, orthogonal wedges in welded contact. This RS wave is essentially a Stoneley type wave[29] propagating along the geometry described above.

The RS wave is theoretically very interesting and gives rise to several important discoveries in the type of waveforms propagated along coupled quarter-spaces. However, the RS range of existence only extends from 0 to 0.3 for ratios of the Lamé constants ($\mu 2/\mu 1$) and densities ($\rho 2/\rho 1$).[28] RS waves do not exist when the two media are the same, similar to the behavior of a Stoneley wave.[29] This limitation on the existence of the RS waves decreases the possible materials in the lab or field that could be used to experimentally verify this waveform.

In this paper, a theoretical and experimental study of coupled wedge waves, along a non-welded contact, was performed for two orthogonal quarter-spaces in contact made of isotropic and anisotropic materials. The theory predicts a dispersive wave that depends on the specific stiffnesses of the contact. The velocity of this coupled wedge wave (CWW) ranges continuously from the WW velocity at low stress to the Rayleigh velocity at high stress. This CWW exists for two quarter-spaces even when the material properties of the quarter-spaces are the same, unlike the RS wave. Since CWWs are able to exist when the two media are the same, CWWs can be used to characterize surface fractures on the laboratory and field scales.

An experimental study was also performed on two isotropic aluminum cubes and two anisotropic aluminum bars, under normal applied load. The measured waves were observed to propagate at velocities within the theoretically predicted range for CWWs and indeed exhibited the dispersive trend predicted by the theory.

II. THEORY

The theoretical derivation of CWWs along a non-welded contact between two quarter-spaces is based on the

a)Author to whom correspondence should be addressed. Electronic mail: ljpn@purdue.edu

derivation approach used for RS waves.[28] In this section, the derivation of coupled wedge waves is described by assuming the interface can be represented as a non-welded contact,[30] i.e., the stress across the interface is continuous but the displacements are not. These boundary conditions lead to the existence of CWWs even when the material properties of the two quarter-spaces are the same, unlike the RS wave. The theory is derived in general in the following sections and the appendixes contain the isotropic and anisotropic material parameters.

A. Problem geometry

The geometry is defined such that an intersection exists on the x_1-x_3 plane at $x_2 = 0$, between two media (Fig. 1). The fracture is modeled as perfectly smooth for $x_3 > 0$. Medium 1 exists in the quarter-space $x_1 > 0$, $x_2 > 0$, $x_3 > 0$, and medium 2 exists in the quarter-space defined by $x_1 > 0,\ x_2 < 0,\ x_3 > 0$.

A free surface exists on the x_1-x_2 plane at $x_3 = 0$. Medium 1 has a mass density $\rho^{(1)}$ and elastic moduli $C^{(1)}_{\alpha,\beta,\mu,\nu}$. The lowercase greek letters indicate the Cartesian indices (i.e., $\alpha,\ \beta,\ \mu,\ \nu = 1, 2, 3$ for the x_1, x_2, x_3 direction, respectively), and the superscript indicates the medium. Similarly, the mass density $\rho^{(2)}$ and elastic moduli $C^{(2)}_{\alpha,\beta,\mu,\nu}$ correspond to medium 2. The CWW solution is derived for the general case when the two media have different material properties. However, the theoretical and experimental results presented here demonstrate that CWWs exist even when the material properties of the two media are the same.

B. Setting up the problem

Throughout the theoretical section, the same variables and notation used by Sokolova *et al.*[28] will be implemented. For waves propagating along the intersection (Fig. 1), the displacement and stress fields are assumed to have the following form:

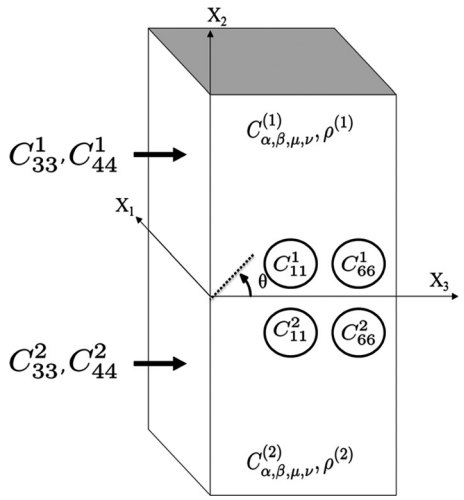

FIG. 1. A single fracture exists along the x_1-x_3 plane at $x_2 = 0$. The wave propagates at $x_2 = x_3 = 0$ in the x_1 direction. θ defines the shear wave transducer polarization angle. The circles and the arrows indicate the direction of the wave propagation to obtain the values of the respective elastic constants (e.g., C_{33} and C_{11}).

$$u_\alpha(x_1, x_2, x_3; t) = e^{i(kx_1-\omega t)}\tilde{U}_\alpha(x_2, x_3|k) + e^{-i(kx_1-\omega t)}\tilde{U}^*_\alpha(x_2, x_3|k), \quad (1)$$

and

$$T_{\alpha,\beta}(x_1, x_2, x_3; t) = e^{i(kx_1-\omega t)}\tilde{T}_{\alpha,\beta}(x_2, x_3|k) + e^{-i(kx_1-\omega t)}\tilde{T}^*_{\alpha,\beta}(x_2, x_3|k), \quad (2)$$

where k is the wave vector ($k = \omega/v$), ω is the frequency, t is the time, $\tilde{U}_\alpha$ are the displacement amplitudes, $\tilde{T}_{\alpha,\beta}$ are the stress amplitudes and the greek subscripts ($\alpha,\ \beta$) represent the direction (i.e., $\alpha = 1, 2, 3$ corresponds to x_1, x_2, x_3). The $x_3\,|\,k$ symbol means the function also has a dependence on k. The equations of motion can be written in terms of the displacement and stress as

$$\rho\frac{\partial^2 u_\alpha}{\partial t^2} = \sum_{\beta=1}^{3}\frac{\partial T_{\alpha\beta}}{\partial x_\beta}, \quad (3)$$

where ρ is the density. The stress tensor is then written in terms of the strains and elastic moduli as

$$T_{\alpha\beta} = \sum_{\mu\nu=1}^{3} C_{\alpha,\beta,\mu,\nu}\frac{1}{2}\left(\frac{\partial u_\mu}{\partial x_\nu} + \frac{\partial u_\nu}{\partial x_\mu}\right), \quad (4)$$

such that after simplification

$$\tilde{T}^{(1/2)}_{\alpha\beta}(x_2, x_3\,|\,k) = \sum_{\mu,v=1}^{3} C^{(1/2)}_{\alpha\beta,\mu,v} D_v(k)\tilde{U}^{(1/2)}_\mu(x_2, x_3\,|\,k), \quad (5)$$

where the D operators are defined as

$$D_1(k) = ik,\ D_2(k) = \frac{\partial}{\partial x_2},\ D_3(k) = \frac{\partial}{\partial x_3}. \quad (6)$$

Applying Eqs. (1) and (2) to the equations of motion yields

$$-\rho\omega^2\tilde{U}_\alpha = \sum_{\beta,\mu,\nu=1}^{3} D_\beta(k) C_{\alpha,\beta,\mu,\nu} D_\nu(k)\tilde{U}_\alpha. \quad (7)$$

The geometry of a single wedge is a quarter plane extending from 0 to ∞ and leads naturally to an expansion extending over the same region. Laguerre polynomials, which are orthonormal from $[0,\ \infty)$, are written as orthonormal basis functions and used in a linear series to represent the displacement amplitudes as[1]

$$\tilde{U}^{(1/2)}_\alpha(x_2, x_3|\,k) = \sum_{m,n=0}^{\infty} a^{(\alpha,1/2)}_{mn}\phi_m(\pm kx_2)\phi_n(kx_3), \quad (8)$$

where

$$\phi_a = e^{-x/2}\frac{L_a(x)}{a!},\ L_a(x) = e^x\frac{d^a}{dx^a}(e^{-x}x^a). \quad (9)$$

The a_{mn} terms are the coefficients of the expansion and L_a is the Laguerre polynomial. This expansion [Eq. (8)] is inserted

into the equations of motion [Eq. (7)], multiplied by $\phi_p(\pm kx_2)\phi_q(kx_3)$ and integrated over each quarter-space such that the advantage of orthonormality is used. With the use of the identity

$$\int_0^{\pm\infty} \phi_a(\pm kx)\phi_b(\pm kx)\mathrm{d}x = \pm\frac{\delta_{ab}}{k}, \tag{10}$$

and

$$\delta_{ab} = \begin{cases} 1 & \text{if } a = b \\ 0 & \text{if } a \neq b, \end{cases} \tag{11}$$

the equations of motion reduce to

$$\begin{aligned} -\rho^{(1/2)}v^2 \sum_{m,n=0}^{\infty} a_{m,n}^{(\alpha,1/2)}\delta_{pm}\delta_{qn} \\ = \pm\sum_{\beta=1}^{3} D_\beta(k)\int_0^{\infty}\int_0^{\pm\infty} \tilde{T}_{\alpha,\beta}^{(1/2)}(x_2, x_3\,|k) \\ \times \phi_p(\pm kx_2)\phi_q(kx_3)\mathrm{d}x_2\mathrm{d}x_3. \end{aligned} \tag{12}$$

Equation (12) is solved using integration by parts and the definition of the stress amplitude at the interface put forth by Sokolova *et al.*,[28]

$$\tau_n^{(\alpha)} \equiv \int_0^{\infty} \phi_n(kx_3)\tilde{T}_{\alpha,2}(0, x_3|k)\mathrm{d}x_3. \tag{13}$$

The resulting relation is

$$\begin{aligned} \sum_{\mu=1}^{3}\sum_{m,n=0}^{\infty}[M_{p,q,m,n}^{(\alpha,\mu,1/2)} - \rho^{(1/2)}v^2\delta_{\alpha\mu}\delta_{pm}\delta_{qn}]\; a_{mn}^{(\mu,1/2)} \\ = \mp\phi_p(0)\tau_q^{(\alpha,1/2)}, \end{aligned} \tag{14}$$

where **M**, which is a Hermitian matrix related to the elastic tensor, is defined in the appendixes for both isotropic and anisotropic media.

Defining the eigenvalues of **M** as λ and the components of the eigenvectors as V_{mn}, the displacement amplitudes, a_{mn}, are written using the similarity transformation. For Hermitian matrices, the similarity transformation is comprised of a diagonal matrix of eigenvalues and two matrices of the concatenation of eigenvector components. Applying the identity matrix (i.e., $\bar{\mathbf{Q}}\bar{\mathbf{Q}}^* = \bar{\mathbf{I}}$, where $\bar{\mathbf{Q}}$ is unitary) to each side of the first term in Eq. (14)

$$\begin{aligned} \bar{\mathbf{Q}}\bar{\mathbf{Q}}^*\sum_{\mu=1}^{3}\sum_{m,n=0}^{\infty}[M_{p,q,m,n}^{(\alpha,\mu,1/2)} - \rho^{(1/2)}v^2\delta_{\alpha\mu}\delta_{pm}\delta_{qn}] \\ \times \bar{\mathbf{Q}}\bar{\mathbf{Q}}^* a_{mn}^{(\mu,1/2)} = \mp\tau_q^{(\alpha,1/2)}, \end{aligned} \tag{15}$$

and making use of the similarity transformation yields

$$\sum_{m=0}^{\infty} a_{m,n}^{(\alpha,1/2)} = \mp\sum_{\beta=1}^{3}\sum_{q=0}^{\infty} G_{nq}^{(\alpha,\beta,1/2)}\tau_q^{(\beta,1/2)}, \tag{16}$$

where

$$\begin{aligned} G_{nq}^{(\alpha,\beta,1/2)} = \sum_{j=1}^{j_{\max}} \frac{Q_n^{(\alpha,1/2)}(j)Q_q^{(\beta,1/2)*}(j)}{\lambda(j) - \rho^{(1/2)}v^2}, \\ j_{\max} = 3(m_{\max}+1)(n_{\max}+1) \end{aligned} \tag{17}$$

and

$$Q_n^{(\alpha,1/2)}(j) = \sum_{m=0}^{m_{\max}} V_{mn}^{(\alpha,1/2)}(j). \tag{18}$$

Here $m_{\max}$ $(=n_{\max})$ refers to the number of expansions performed in Eq. (8).

The expansion coefficients are related to the amplitude at the interface ($x_2 = 0$), by

$$U_n^{(\alpha,1/2)} \equiv k\int_0^{\infty} \phi_n(kx_3)\,\tilde{U}_\alpha^{(1/2)}(0, x_3|k)\,\mathrm{d}x_3. \tag{19}$$

Using Eqs. (8) and (10), Eq. (19) is rewritten as

$$U_n^{(\alpha,1/2)} = \sum_{m=0}^{\infty} a_{m,n}^{(\alpha,1/2)}. \tag{20}$$

Substituting Eq. (20) into Eq. (16) yields

$$U_n^{(\alpha,1/2)} = \mp\sum_{\beta=1}^{3}\sum_{q=0}^{\infty} G_{nq}^{(\alpha,\beta,1/2)}\tau_q^{(\beta,1/2)}, \tag{21}$$

and is re-arranged to give

$$\mathbf{G}^{(\alpha,\beta,1/2)-1}\,\mathbf{U}^{(\alpha,1/2)} = \mp\,\boldsymbol{\tau}^{(\beta,1/2)}. \tag{22}$$

Equation (22) defines the relationship between the displacements and stresses at the interface ($x_2 = 0$, Fig. 1). **G** contains the full set of elastic constants, $C_{\alpha,\beta,\mu,\nu}$.

C. Boundary conditions

Previous theoretical work on CWWs assumed a welded contact between the two media.[25–28] In this study, the interface is assumed to be non-welded, i.e., continuity in stress and a discontinuity in displacement. The discontinuity in displacement is assumed to be proportional to stress and inversely proportional to the specific stiffness of the interface.[30–33] The boundary conditions across the interface ($x_1 \geq 0,\ x_2 = 0,\ x_3 \geq 0$) are

$$\tilde{U}_\alpha^{(1)} - \tilde{U}_\alpha^{(2)} = \frac{\tilde{T}_{\alpha,2}^{(1)}}{\kappa_\alpha},\ \alpha = 1, 2, 3, \tag{23}$$

and

$$\tau^{(\beta,1)} = \tau^{(\beta,2)},\ \beta = 1, 2, 3, \tag{24}$$

where κ_α is the specific stiffness in the α direction. The specific stiffness of an interface, or fracture, depends on the amount and spatial distribution of contact area between two surfaces and is a function of stress.[34,35] In the following section, these boundary conditions were used to derive the

velocity for CWWs that propagate along the edge of a non-welded interface (Fig. 1).

D. Application of the boundary conditions

Applying the stress boundary condition [Eq. (24)] to Eq. (22) produces

$$\mathbf{G}^{-1(\alpha,\beta,1)}\,\mathbf{U}^{(\alpha,1)} + \mathbf{G}^{-1(\alpha,\beta,2)}\,\mathbf{U}^{(\alpha,2)} = 0\,, \tag{25}$$

where $\mathbf{G}^{-1}$ is the inverse of $\mathbf{G}$. The displacement discontinuity boundary condition [Eq. (23)] is multiplied by $\phi_l(kx_3)$ and integrated over the quarter-space, with the use of Eqs. (13), (19), and (20) yielding

$$\frac{1}{k}[U_n^{(\alpha,1)} - \ U_n^{(\alpha,2)}] = \frac{1}{\kappa_\alpha}\tau_n^{(\alpha,1)}. \tag{26}$$

Solving Eq. (26) for U_n and substituting into Eq. (25) leads to

$$-\mathbf{G}^{-1(\alpha,\beta,1)}\left[\frac{k}{k_\alpha}\tau_n^{(\alpha,2)} + \mathbf{U}_n^{(\alpha,2)}\right] = \mathbf{G}^{-1(\alpha,\beta,2)}\mathbf{U}_n^{(\alpha,2)}, \tag{27}$$

$$\left[\mathbf{G}^{-1(\alpha,\beta,1)}\mathbf{G}^{-1(\alpha,\beta,2)}\frac{k}{k_\alpha} + \mathbf{G}^{-1(\alpha,\beta,1)} + \mathbf{G}^{-1(\alpha,\beta,2)}\right]\mathbf{U}_n^{(\alpha,2)} = 0. \tag{28}$$

Equation (28) yields an eigenvalue problem that has solutions when

$$\det\left[\mathbf{G}^{-1(\alpha,\beta,1)}\mathbf{G}^{-1(\alpha,\beta,2)}\frac{k}{k_\alpha} + \mathbf{G}^{-1(\alpha,\beta,1)} + \mathbf{G}^{-1(\alpha,\beta,2)}\right] = 0. \tag{29}$$

Equation (29) is a secular equation relating the stress, frequency, velocity, and elastic constants to each other for the problem geometry (Fig. 1) using the boundary conditions in the previous section. The secular equation [Eq. (29)] is a function of frequency and stiffness as expected for problems using displacement discontinuity boundary conditions.[30–32]

E. Conditions for specific stiffness

When $\kappa_\alpha \to \infty$ $(\alpha = 1, 2, 3)$ the solution for CWWs reverts to the RS wave, as long as the material parameters are within the region of existence for RS waves,[28] as is required for welded interfaces. When $\kappa_\alpha \to 0$ $(\alpha = 1, 2, 3)$ which is a free surface boundary condition, $\mathbf{G}^{-1(\alpha,\beta,1)} \to 0$ while $1/\kappa_\alpha \to \infty$ canceling the first and second terms in Eq. (29). This leaves the determinant $\det[\mathbf{G}^{-1(\alpha,\beta,2)}] = 0$ which is the equation for a WW.[1]

The solution for a CWW depends on the specific stiffnesses: κ_x, κ_y, κ_z of the contact plane. Previous studies on the ratio of shear to normal stiffness have been performed in the lab and in the field.[36,37] Theoretically, it has been hypothesized to be 1. In this study, for simplicity, κ_α was assumed to be equal in the $\alpha = 1,\ 2$ directions. Due to the presence of a free surface in the $\hat{x}_3$ direction, the stiffness term in that direction (i.e., k/κ_3) is multiplied by zero stress, and so the stiffness is set to $\kappa_3 = \infty$ to be consistent with the free surface. Previous work showed that the displacement should decay exponentially in the x_3 direction as a function of wavelength.[2] Other surface waves, such as Rayleigh, Stoneley, and Scholte waves, have been shown to decay harmonically [see Ref. 38 and references within].

III. NUMERICAL ANALYSIS

A. Isotropic case

A numerical study was performed to determine the range of existence and velocity of CWW modes as a function of specific stiffness and frequency when the material properties of medium 1 and medium 2 are equal. The transformation

$$\hat{u}_1 = i\tilde{u}_1,\ \hat{u}_2 = \tilde{u}_2,\ \hat{u}_3 = \tilde{u}_3, \tag{30}$$

was used to make the $\mathbf{M}$ and $\mathbf{G}$ matrices [in Eqs. (17) and (A1)] real, as was first used in the derivation of WWs by Maradudin[1] and based on the proof set forth by Ludwig *et al.*[39] This transformation changes the operator $D_1(k)$ in Eq. (6) such that $D_1(k) = -k$. Note that only the $\alpha = 1$ terms are affected by the transformation in Eq. (30) and thus only terms M_{12}, M_{13}, M_{21} and M_{31} are altered. That is

$$\begin{aligned} M_{12} &\to iM_{12},\\ M_{13} &\to iM_{13},\\ M_{21} &\to -iM_{21},\\ M_{31} &\to -iM_{31}. \end{aligned} \tag{31}$$

The physical parameters used to solve Eq. (29) are listed in Tables I and II and are based on the properties of the isotropic aluminum cubes used in the experiments (see Sec. IV). Theoretical velocities for the CWW were found for a range of specific stiffnesses and a range of frequencies using $n_{\max} = m_{\max} = 15$, which defined the number of Laguerre polynomials used in the expansion of the displacement.

Figure 2 shows the numerical results of normalized CWW phase velocity as a function of normalized frequency. The CWW velocity is normalized by the Rayleigh wave velocity, while the frequency is normalized by the ratio of the specific stiffness, κ to the seismic impedance, Z.

When the fracture stiffness on the interface is small ($\omega Z/\kappa > 1e4$ in Fig. 2) the velocity is that of a single wedge wave. As the fracture stiffness on the interface approaches zero, the contact area between the surfaces decreases and the WWs are no longer coupled, thus leaving the velocity of a single wedge wave. As the stiffness increases, the wedges couple through points of contact. The CWW velocity increases continually as the stiffness increases until the interface is in welded

TABLE I. Sample dimensions for directions as shown in Figure 1. All sizes have an uncertainty of ±0.3 mm.

Direction	Isotropic Aluminum	Anisotropic Aluminum
X_1 (m)	0.3025	0.2978
X_2 (m)	0.3025	0.0762
X_3 (m)	0.3025	0.0762

TABLE II. Measured isotropic and anisotropic aluminum parameters used in the numerical analysis. The first parenthesis is the direction the velocity was measured in, the second is the unit.

Parameter	Isotropic Aluminum	Anisotropic Aluminum
ρ (kg/m^3)	2700	2717
C_{11} (Pa)	1.0332×10^{11}	8.8750×10^{10}
C_{12} (Pa)	5.1960×10^{10}	4.1460×10^{10}
C_{13} (Pa)	5.1960×10^{10}	3.7000×10^{10}
C_{33} (Pa)	1.0332×10^{11}	1.0545×10^{11}
C_{44} (Pa)	2.5680×10^{10}	2.5607×10^{10}
C_{66} (Pa)	2.5680×10^{10}	2.3645×10^{10}
$n_{\max} = m_{\max}$	15	15
Shear Velocity (x_1) (m/s)	3084.5 ± 2.5	3070.0 ± 2.5
Shear Velocity (x_2, x_3) (m/s)	3084.5 ± 2.5	2950.0 ± 2.5
Rayleigh Velocity (x_1) (m/s)	2890.0 ± 10.0	2900.0 ± 1.0
Rayleigh Velocity (x_2, x_3) (m/s)	2890.0 ± 10.0	2780.0 ± 1.0
Wedge Velocity (m/s)	2815.0 ± 5.0	2840.0 ± 10.0
P- Velocity (x_1) (m/s)	6185.6 ± 2.5	6230.0 ± 2.5
P- Velocity (x_2, x_3) (m/s)	6185.6 ± 2.5	5715.3 ± 2.5

contact. At that stiffness ($\omega Z/\kappa < 1$ in Fig. 2), the two media form a half space, that gives rise to a Rayleigh wave.[40] Whether or not the interface appears welded will depend on the frequency of the signal. For a given stiffness, low frequency components of a CWW signal will propagate with a greater velocity than high frequency components.

B. Anisotropic case

When the materials under observation are anisotropic, assumption of isotropy in velocity will lead to a miscalculation of the velocity as a function of stiffness. To show this effect, the velocities for two different directions in the anisotropic aluminum (Table II) were used in the isotropic theory, separately, and compared to the anisotropic analysis (Fig. 3). The shear and compressional wave velocities from the x_1 direction were applied to the isotropic CWW theory (Appendix A). If the anisotropic parameters only from the x_1 direction of the anisotropic medium were used in the isotropic theory, then a velocity range slightly lower than the wedge velocity was obtained (partially dashed line in Fig. 3). If only the x_2 direction parameters (dashed line Fig. 3) were used instead, then the velocity range is even lower than the correct range based on anisotropic theory. When the fully anisotropic theory is applied (Appendix B), the velocity range is in the expected range for CWWs (solid line in Fig. 3). Note that the error bars in Fig. 3 are the range of velocities measured for all the anisotropic sample surfaces and wedges, respectively.

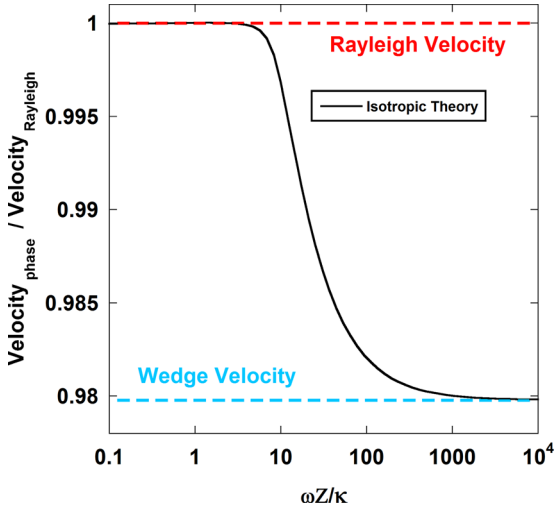

FIG. 2. (Color online) Phase velocity of the coupled wedge mode normalized by the Rayleigh velocity as a function of $\omega/Z\kappa$, where $\omega = 2\pi f$, $Z = v_{\text{shear}}\rho$ and κ is stiffness. This result is for $\kappa_{x_1} = \kappa_{x_2}$ and $\kappa_{x_3} = \infty$.

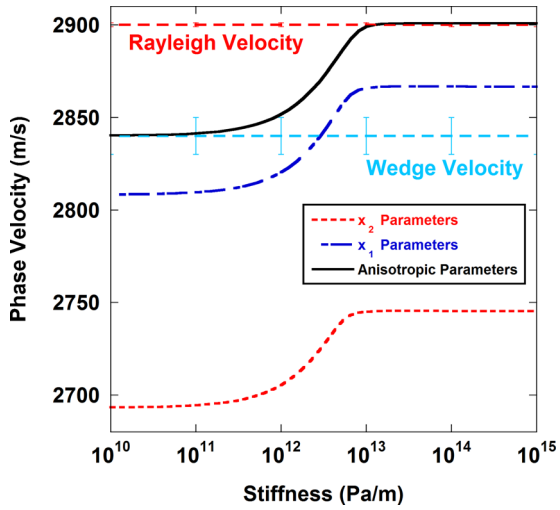

FIG. 3. (Color online) Comparison of isotropic and anisotropic theory. The x_1 and x_2 velocities (see Table II) were applied to the isotropic theory, separately. For all curves $\kappa_{x_1} = \kappa_{x_2}$, $\kappa_{x_3} = \infty$.

The observed difference between the isotropic and anisotropic theory is significant because not accounting for a sample anisotropy of only 4% resulted in a predicted theoretical velocity that did not match the data. This comparison indicates the high sensitivity of CWWs to the anisotropy of the sample.

IV. EXPERIMENTAL SETUP

Experiments were performed on two isotropic aluminum cubes and two anisotropic aluminum bars. The sample dimensions are listed in Table I. Long samples were used to separate the wedge and Rayleigh waves which propagate at velocities within ~2% of each other for wedges of 90°.[1] All the samples were machined smooth on all sides to a roughness of ±25 μm.

Piezoelectric contact transducers (Olympus-Panametrics $V103$ and $V153$) with a central frequency of 1 MHz were used to send and receive compressional (P) and shear (S) waves. Transducer arrays were held in a platen for mounting on the sample. Honey (with 8.75% of the water removed through heating at 90 °C for ~120 min) was used as a couplant between the transducer and the sample. The array contained (a) two S-wave transducers that were used to sample the free surface, (b) two S-wave transducers transducers to sample the bulk, (c) one S-wave transducer to sample the interface, and (d) one S-wave transducer to sample the wedge region.

The source transducers were excited with a square wave pulse of 400 V with a repetition rate of 1 kHz from an Olympus 5077PR pulse generator. After propagating through

the sample, the signals were received by the receiver transducers and recorded using a National Instrument PXI-1042 controller with a PXI-5122 digitizer and stored on a computer for later analysis. The $V153$ and $V103$ transducers were used to measure the bulk S-waves and bulk P-waves through each sample, respectively. The bulk, Rayleigh, and wedge wave velocities are listed in Table II.

As discovered previously by DeBilly *et al.*,[6] the ability to sense a wedge wave depends on the polarization of the S-wave transducer. When the transducer is polarized perpendicularly to the line bisecting the wedge (i.e., $\theta = 45^\circ$ for medium 2 in Fig. 1), the signal has the largest amplitude (wedge in Fig. 4). The smallest amplitude was observed when the wave polarization was parallel (i.e., $\theta = 135^\circ$ for medium 2 in Fig. 1) to the bisecting line (non-wedge in Fig. 4). The Rayleigh and bulk S-wave are also shown in Fig. 4 for comparison.

The polarization used to measure the coupled wedge mode was $\theta = 0^\circ$ from the horizontal as shown in Fig. 1. This angle was chosen based upon the displacement amplitudes extracted from the isotropic theory for coupled wedge waves.

A single axis Instron 444 kN load frame was used to apply a normal load to the fracture, i.e., along the x_2 direction, to change the contact area between the two blocks and thus the specific stiffness of the interface. An Instron Model 59-*R*8100*BTE* controlled by Bluehill 3 software was used to control and continuously monitor the load. The applied load ranged from 0 to 400.3 kN and was evenly distributed by placing spacers above the sample. For each 2.22 kN increment in load, the load was held constant while 30 signals were acquired and averaged at each transducer location.

V. RESULTS AND DISCUSSION

Signals were recorded on the bulk, the wedge, and surface of each sample. For isotropic aluminum, the signals were independent of the cube face used and determined to be the same in each block. For the anisotropic aluminum, the waveforms varied in each sample and in each direction due to the anisotropy. CWWs were observed and found to decrease in arrival time as the load was increased for both the isotropic and anisotropic samples. The CWW waveforms are shown in Figs. 5 and 6 for low (0–22 kN), medium (111.2–222.4 kN), and high (400.3 kN) applied loads on both the isotropic and anisotropic samples. Rayleigh and wedge waves are also shown for reference in the same figures. Note that the CWW is similar to the WW at 0 kN and approaches the Rayleigh wave at 400.3 kN.

Wavelet analysis[41] was performed to determine the group arrival time for a given frequency. From this analysis,

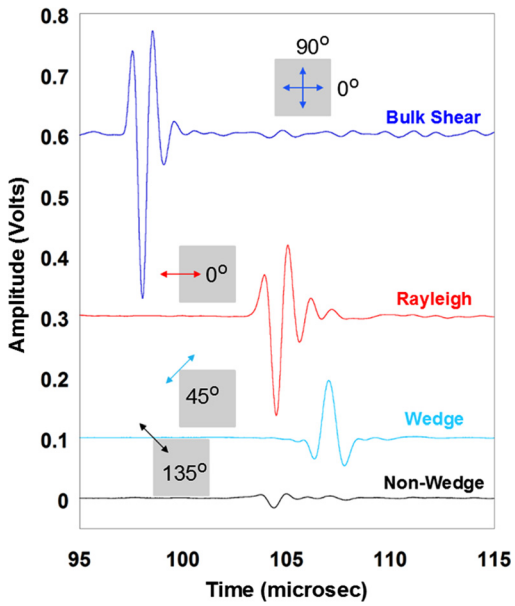

FIG. 4. (Color online) Received waveforms from isotropic aluminum showing the bulk, Rayleigh, wedge, and non-wedge polarization waves.

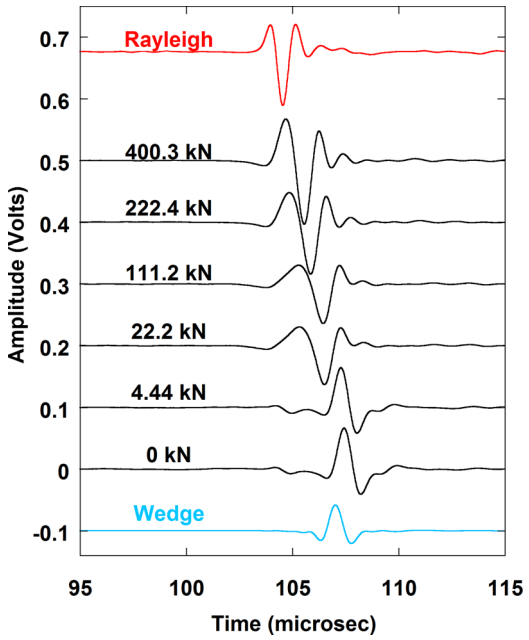

FIG. 5. (Color online) Waveforms from the isotropic aluminum sample for the coupled wedge (0 kN to 400.3 kN), the single wedge and Rayleigh mode.

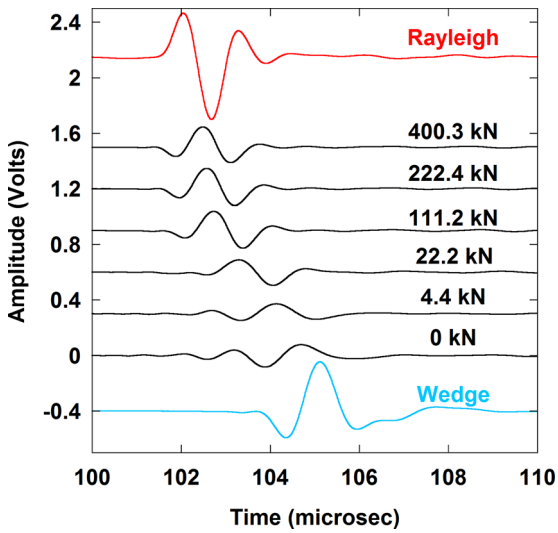

FIG. 6. (Color online) Waveforms from the anisotropic aluminum sample for the coupled wedge (0 kN to 400.3 kN), the single wedge and Rayleigh mode.

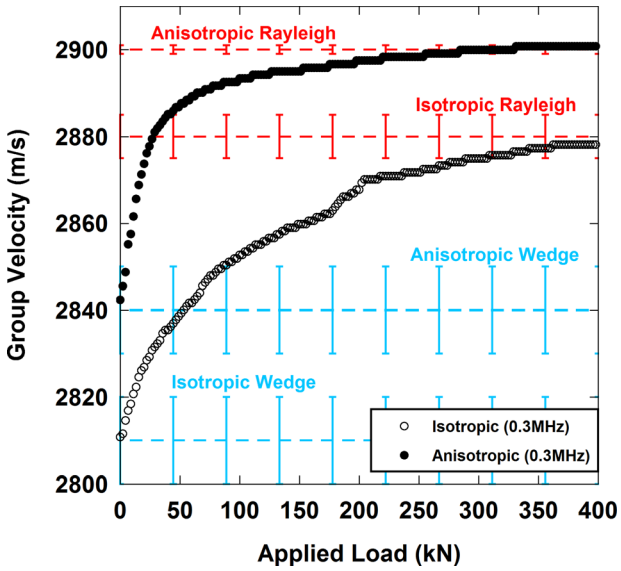

FIG. 7. (Color online) Experimental group velocities at 0.3 MHz for both the isotropic and anisotropic aluminum samples.

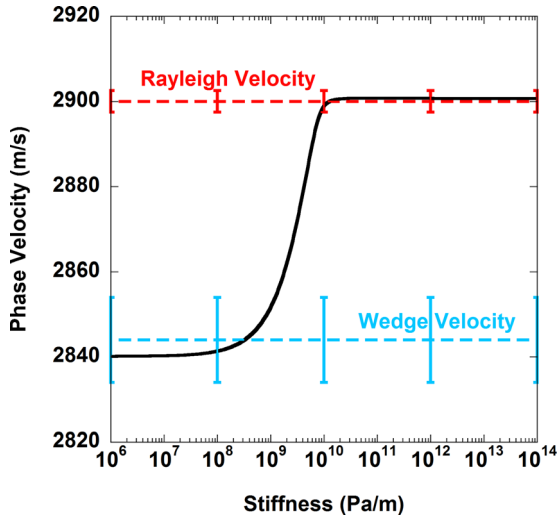

FIG. 9. (Color online) Phase velocity of the anisotropic coupled wedge mode as a function of stiffness. The error bars on the wedge and Rayleigh velocity are the range of values for the anisotropic samples used in this experiment (see Table II). This result is for $\kappa_{x_1} = \kappa_{x_2}$ and $\kappa_{x_3} = \infty$.

a frequency of 0.3 MHz was used to calculate the group velocity. Group velocities for both the isotropic and anisotropic samples were calculated and are shown in Fig. 7 as a function of applied load. The same method was used to calculate the group wedge and group Rayleigh wave velocity, which are also shown in Fig. 7 by the dashed lines. As the normal load increased, the coupling between the wedges increased, resulting in an increase in velocity from the single wedge wave velocity towards the Rayleigh wave velocity. The uncertainties in velocity are within the size of the symbols for the experimental data. The error bars on the wedge and Rayleigh velocities of Fig. 7 give the range of values for all sample surfaces and wedges (see Table II).

As discussed in Sec. II E, the ratio of shear to normal stiffness is assumed to be 1. However, from experimental studies, this can vary and affect the interpretation of the specific stiffness. To show the variation in the predicted velocity, stiffness, and frequency, the isotropic CWW theory was explored for different shear to normal stiffness ratios. Figure 8 shows the velocity as a function of normalized frequency for different shear (κ_{x1}) to normal (κ_{x2}) stiffness ratios. Since the horizontal axis has been normalized, the shift in the velocity curves is purely from the stiffness ratio. For smooth fractures, as in the experimental section of this paper, the assumption of the stiffness ratio equaling 1 is a good approximation. For more complicated fracture planes and other rock fractures, this ratio will need to be explored further and carefully measured to ensure a good estimate of the specific stiffness for the interface where the wedges are coupled.

The group velocities in Fig. 7 were used in both the isotropic and anisotropic theory (Figs. 2 and 9) to obtain an estimate for the specific stiffness of the surface fracture, assuming a shear to normal stiffness ratio of 1. The estimated stiffness for a frequency of 0.3 MHz is shown in Fig. 10 as a function of applied load. The range of stiffness

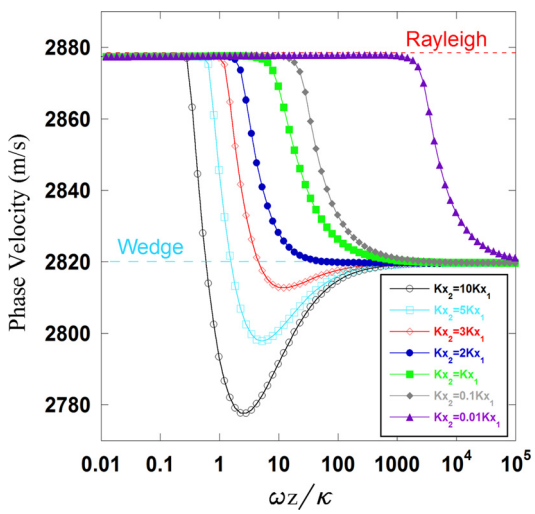

FIG. 8. (Color online) Theoretical phase velocities, for different shear to normal stiffness ratios, as a function of normalized stiffness. Here ω is the frequency, Z is the impedance, and κ is the specific stiffness κ_{x_1}.

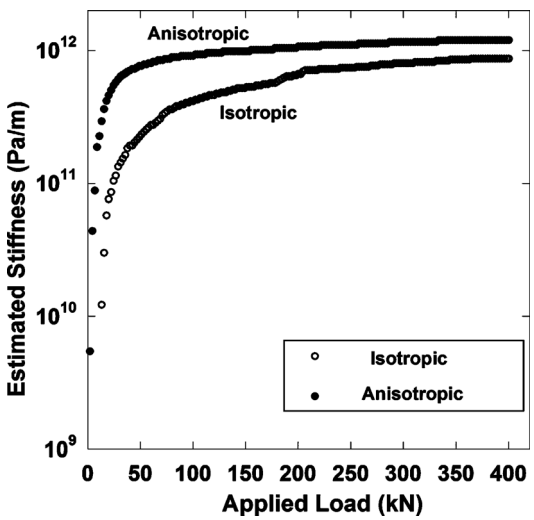

FIG. 10. The group velocities from Fig. 7 were used to estimate the specific stiffness along the interface for both the isotropic and anisotropic samples at 0.3 MHz.

values obtained is in the previously observed range for aluminum samples measured using interface waves at high frequency.[42]

VI. CONCLUSION

This study investigated the existence of coupled wedge waves (CWWs), both theoretically and experimentally. These elastic waves propagate along the intersection of two quarter-spaces, each supporting a WW mode, coupled through displacement discontinuity boundary conditions. The velocity of the CWW ranges continuously from the WW velocity to the Rayleigh wave velocity and depends on the interface stiffness and frequency. For any surface fracture, the two wedge waves, one from each medium, can exist independently, when there is no contact between the wedges, i.e., for uncoupled wedges. When stress is applied to the media, causing the two wedges to come into partial contact, the wedges couple to form the CWW. It can exist whether the material properties of the two quarter-spaces are the same or different, unlike a Rayleigh–Stoneley wave which can only exist when the two media are different. This broadens the applicability of the CWW to applications on the lab and field scale such as surface fractures in rock.

CWWs were shown to exist by using a Laguerre polynomial expansion in displacement, applying displacement discontinuity boundary conditions, and using a numerical approximation to calculate the CWW velocity region. Numerical analysis demonstrated that at low stiffness the coupled wedge wave should propagate at the WW velocity and for high stiffness at the Rayleigh velocity. Both the isotropic and anisotropic cases were analyzed and equations were derived for each. The theoretical derivation is independent of size and can be expanded to the field scale for a wide range of frequencies, making the CWW more applicable.

The experimental study was performed on aluminum cubes and bars with orthogonal wedges. The isotropic theory was found to be in good agreement with the experimental isotropic sample but was unable to predict the velocity range in the anisotropic sample, even with 4% anisotropy. When the anisotropic theory was then applied, the theoretical velocity range was found to predict the experimentally observed velocity range exactly, indicating a theoretical model that is highly sensitive to anisotropy. The dispersive behavior of CWW enabled the stiffness of the interface to be estimated and was found to be in good agreement with previous work performed on aluminum at high frequency. These results indicate that the CWW does exist along the contact between two quarter-spaces in contact and is sensitive to the load. The experimental study verified that the waveforms observed were in fact load dependent and indicated that at the wedge tips, the bond was not welded but was in the displacement discontinuity regime.

ACKNOWLEDGMENTS

The authors wish to acknowledge support of this work by the Geosciences Research Program, Office of Basic Energy Sciences US Department of Energy (DE-FG02-09ER16022), the Geo-Mathematical Imaging Group at Purdue University and A. P. Mayer for his helpful discussion regarding the theory.

APPENDIX A: ISOTROPIC THEORY

Although the mathematical formulation from the theory section in this paper is based on the work done by Sokolova *et al.*,[28] there are several equations which were not explicitly shown in their theory section which aid greatly in solving for the velocity of CWWs. For the isotropic case, using the transformation described in Sec. III [Eq. (30)], the matrix **M** is necessary to the solution but can be difficult to formulate without the following relationships.

The definition of **M**, which is size $(m_{\max}+1)^2 \times (m_{\max}+1)^2$, is[28]

$$M_{pq,mn}^{(\alpha,\mu,1/2)} = \pm \sum_{\beta,v=1}^{3} \int_0^{\infty} \int_0^{\pm\infty} [D_\beta(k)\phi_p(\pm kx_2)\phi_q(kx_3)]^* \times C_{\alpha\beta\mu w}^{(1/2)} [D_v(k)\phi_m(\pm kx_2)\phi_n(kx_3)] dx_2 dx_3. \tag{A1}$$

To solve Eq. (A1), there are three possible integrals involving the Laguerre polynomials, ϕ, that need to be implemented. The three integrals are Eq. (10),

$$\int_0^{\pm\infty} \phi_a(\pm kx)\frac{\partial}{\partial x}\phi_b(\pm kx)dx = -\Theta(b-a) + \frac{\delta_{ab}}{2} \equiv \psi_{a,b}, \tag{A2}$$

where Θ is a step function defined by

$$\Theta(f) = \begin{cases} 0 & \text{if } f < 0 \\ 1 & \text{if } f \geq 0, \end{cases} \tag{A3}$$

and

$$\int_0^{\pm\infty} \frac{\partial}{\partial x}[\phi_a(\pm kx)]\frac{\partial}{\partial x}[\phi_b(\pm kx)]dx = \pm k\left[\min(a,b) + \frac{1}{2} - \frac{\delta_{ab}}{4}\right] \equiv \pm k\Gamma_{a,b}. \tag{A4}$$

Using the above relationships, and the Voigt notation (e.g., $1232 = 64$), the matrix elements of **M** for an isotropic solid are found to be

$$M_{pq,mn}^{(1,1,1/2)} = C_{11}^{(1/2)}\delta_{pm}\delta_{qn} + C_{66}^{(1/2)}\{\delta_{qn}\Gamma_{p,m} + \delta_{pm}\Gamma_{q,n}\}, \tag{A5}$$

$$M_{pq,mn}^{(1,2,1/2)} = \pm[C_{12}^{(1/2)}\delta_{qn}\psi_{p,m} - C_{66}^{(1/2)}\delta_{qn}\psi_{m,p}], \tag{A6}$$

$$M_{pq,mn}^{(1,3,1/2)} = C_{12}^{(1/2)}\delta_{pm}\psi_{q,n} - C_{66}^{(1/2)}\partial_{pm}\psi_{n,q}, \tag{A7}$$

$$M_{pq,mn}^{(2,1,1/2)} = \mp[C_{66}^{(1/2)}\delta_{qn}\psi_{p,m} - C_{12}^{(1/2)}\delta_{qn}\psi_{m,p}], \tag{A8}$$

$$M_{pq,mn}^{(2,2,1/2)} = C_{66}^{(1/2)}\delta_{pm}\delta_{qn} + C_{11}^{(1/2)}\delta_{qn}\Gamma_{m,p} + C_{66}^{(1/2)}\delta_{pm}\Gamma_{q,n}, \tag{A9}$$

$$M^{(2,3,1/2)}_{pq,mn} = \pm[C^{(1/2)}_{12}\psi_{m,p}\psi_{q,n} + C^{(1/2)}_{66}\psi_{p,m}\psi_{n,q}], \tag{A10}$$

$$M^{(3,1,1/2)}_{pq,mn} = -C^{(1/2)}_{66}\delta_{pm}\psi_{q,n} + C^{(1/2)}_{12}\delta_{pm}\psi_{n,q}, \tag{A11}$$

$$M^{(3,2,1/2)}_{pq,mn} = \pm[C^{(1/2)}_{66}\psi_{m,p}\psi_{q,n} + C^{(1/2)}_{12}\psi_{p,m}\psi_{n,q}], \tag{A12}$$

$$M^{(3,3,1/2)}_{pq,mn} = C^{(1/2)}_{66}\delta_{pm}\delta_{qn} + C^{(1/2)}_{66}\delta_{qn}\Gamma_{m,p} + C^{(1/2)}_{11}\delta_{pm}\Gamma_{n,q}. \tag{A13}$$

When Eqs. (A5)–(A13) are used to form matrix **M**, the result is a Hermitian ($\mathbf{M} = \mathbf{M}^{\dagger}$) matrix independent of k. As a numerical example, if the isotropic parameters in Table II are used in the above theory, the velocity of the CWW ranges from 2820 m/s to 2978 m/s.

APPENDIX B: ANISOTROPIC THEORY

For anisotropic materials, a similar approach for solving **M** [Eq. (A1)] is applied, but with a general anisotropic elastic stiffness tensor. For a general orthorhombic medium, the elastic stiffness tensor can be expressed as

$$C^{(1/2)}_{\alpha\beta\mu\nu} = \begin{pmatrix} C_{11} & C_{12} & C_{13} & 0 & 0 & 0 \\ C_{12} & C_{22} & C_{23} & 0 & 0 & 0 \\ C_{13} & C_{23} & C_{33} & 0 & 0 & 0 \\ 0 & 0 & 0 & C_{44} & 0 & 0 \\ 0 & 0 & 0 & 0 & C_{55} & 0 \\ 0 & 0 & 0 & 0 & 0 & C_{66} \end{pmatrix}, \tag{B1}$$

where the Voigt notation has again been utilized. Substituting Eq. (B1) into Eq. (A1) the following matrix terms are found

$$M^{(1,1,1/2)}_{pq,mn} = C^{(1/2)}_{11}\delta_{pm}\delta_{qn} + C^{(1/2)}_{66}\delta_{qn}\Gamma_{m,p} + C^{(1/2)}_{55}\delta_{pm}\Gamma_{n,q}, \tag{B2}$$

$$M^{(1,2,1/2)}_{pq,mn} = \pm[C^{(1/2)}_{12}\delta_{qn}\psi_{p,m} - C^{(1/2)}_{66}\delta_{qn}\psi_{m,p}], \tag{B3}$$

$$M^{(1,3,1/2)}_{pq,mn} = C^{(1/2)}_{13}\delta_{pm}\psi_{q,n} - C^{(1/2)}_{55}\delta_{pm}\psi_{n,q}, \tag{B4}$$

$$M^{(2,1,1/2)}_{pq,mn} = \mp[C^{(1/2)}_{66}\delta_{qn}\psi_{p,m} - C^{(1/2)}_{12}\delta_{qn}\psi_{m,p}], \tag{B5}$$

$$M^{(2,2,1/2)}_{pq,mn} = C^{(1/2)}_{66}\delta_{pm}\delta_{qn} + C^{(1/2)}_{22}\delta_{qn}\Gamma_{m,p} + C^{(1/2)}_{44}\delta_{pm}\Gamma_{q,n}, \tag{B6}$$

$$M^{(2,3,1/2)}_{pq,mn} = \pm[C^{(1/2)}_{23}\psi_{m,p}\psi_{q,n} + C^{(1/2)}_{44}\psi_{p,m}\psi_{n,q}], \tag{B7}$$

$$M^{(3,1,1/2)}_{pq,mn} = -C^{(1/2)}_{55}\delta_{pm}\psi_{q,n} + C^{(1/2)}_{13}\delta_{pm}\psi_{n,q}, \tag{B8}$$

$$M^{(3,2,1/2)}_{pq,mn} = \pm[C^{(1/2)}_{44}\psi_{m,p}\psi_{q,n} + C^{(1/2)}_{23}\psi_{n,q}\psi_{p,m}], \tag{B9}$$

$$M^{(3,3,1/2)}_{pq,mn} = C^{(1/2)}_{55}\delta_{pm}\delta_{qn} + C^{(1/2)}_{44}\delta_{qn}\Gamma_{m,p} + C^{(1/2)}_{33}\delta_{pm}\Gamma_{n,q}. \tag{B10}$$

Here again, **M** is Hermitian and independent of k. If the terms in the elastic stiffness tensor [Eq. (B1)] are made to be isotropic, the matrix elements revert back to the isotropic case derived in Appendix A. This is written for general anisotropy and can be rotated or simplified for different anisotropies.

As an example, if transversely isotropic media were under study, Eq. (B1) would simplify to

$$C^{(1/2)}_{\alpha\beta\mu\nu} = \begin{pmatrix} C_{11} & C_{12} & C_{13} & 0 & 0 & 0 \\ C_{12} & C_{11} & C_{13} & 0 & 0 & 0 \\ C_{13} & C_{13} & C_{33} & 0 & 0 & 0 \\ 0 & 0 & 0 & C_{44} & 0 & 0 \\ 0 & 0 & 0 & 0 & C_{44} & 0 \\ 0 & 0 & 0 & 0 & 0 & C_{66} \end{pmatrix}. \tag{B11}$$

The elastic stiffness terms in Eq. (B11) can be measured experimentally from the S- and P-wave velocities in the three orthogonal directions aligned with the symmetry axis, except for the C_{13} term. This term is a function of the off diagonal compressional velocity, which is difficult to measure. To get an estimate for this term, the Rayleigh velocity, propagating along the same direction as the coupled wedge wave (i.e., x_1 direction in Fig. 1), can be used. Based on the analytic expression put forth by Vinh and Ogden,[43] the Rayleigh velocity, for any anisotropic media, can be written in terms of the C_{11}, C_{33}, C_{13} and C_{55} terms. Vinh and Ogden explicitly worked through expressions for orthotropic media, but a simple substitution based on symmetries set forth by Chadwick,[44] leads to other symmetries such as transversely isotropic media.

[1] A. A. Maradudin, R. F. Wallis, D. L. Mills, and R. L. Ballard, "Vibrational edge modes in finite crystals," Phys. Rev. B **6**(4), 1106–1111 (1972).
[2] P. E. Lagasse, "Analysis of a dispersion free guide for elastic waves," Electron. Lett. **8**, 372–373 (1972).
[3] S. L. Moss, A. A. Maradudin, and S. L. Cunningham, "Vibrational edge modes for wedges with arbitrary interior angles," Phys. Rev. B **8**, 2999–3008 (1973).
[4] M. DeBilly, A. C. Hladky-Hennion, and R. Bossut, "On the localization of the antisymmetric flexural edge waves for obtuse angles," Ultrason. **36**, 995–1001 (1998).
[5] M. DeBilly, A. C. Hladky-Hennion, and R. Bossut, "The effect of imperfections on acoustic wave propagation along a wedge waveguide," Ultrason. **37**, 413–416 (1999).
[6] M. Debilly, "Acoustic technique applied to the measurement of the free edge wave velocity" Ultrason. **34**, 611–619 (1996).
[7] X. Jia and M. DeBilly, "Observation of the dispersion behavior of surface acoustic waves in a wedge waveguide by laser ultrasonics," Appl. Phys. Lett. **61**, 2970–2972 (1992).
[8] R. Adler, M. Hoskins, S. Datta, and B. Hunsinger, "Unusual parametric effects on line acoustic waves," IEEE Trans. Sonics Ultrason. **26**, 345–347 (1979).
[9] A. A. Maradudin, "Edge modes," Jpn. J. Appl. Phys. Suppl. **2**, 871–878 (1974).
[10] A. A. Oliner, "Waveguides for acoustic surface waves: A review," Proc. IEEE **64**, 615–627 (1976).
[11] A. A. Maradudin, "Surface waves," Feskorperprobleme **12**, 1–116 (1981).
[12] E. Sokolova, A. Kovalev, R. Timler, and A. Mayer, "On the dispersion of wedge acoustic waves," Wave Motion **50**, 233–245 (2013).
[13] J. McKenna, G. D. Boyd, and R. N. Thurston, "Plate theory solutions for guided flexural acoustic waves along the tip of a wedge," IEEE Trans. Sonics Ultrason. **3**, 178–186 (1974).
[14] V. V. Krylov, "Distinctive characteristics of guided surface-wave propagation in complex topographic structures," Sov. Phys. Acoust. **33**, 407–411 (1987).
[15] A. A. Maradudin and K. R. Subbaswamy, "Edge localized vibration modes on a rectangular ridge," J. Appl. Phys. **48**, 3410–3414 (1977).

[16]Z. L. Li, I. Achenbach, J. D. Komsky, and Y. C. Lee, "Reflection and transmission of obliquely incident surface waves by an edge of a quarter space: Theory and experiment," J. Appl. Mech. **59**, 349–355 (1992).
[17]A. A. Krushynska, "Flexural edge waves in semi-infinite elastic plates," J. Sound Vib. **330**, 1964–1976 (2011).
[18]V. V. Krylov and A. V. Shanin, "Influence of elastic anisotropy on the velocities of acoustic wedge modes," Sov. Phys. Acoust. **37**, 65–67 (1991).
[19]A. L. Shuvalov and V. V. Krylov, "Localized vibration modes in free anisotropic wedges," J. Acoust. Soc. Am. **107**, 657–660 (2000).
[20]A. D. Boardman, R. Garcia-Molina, A. Gras-Marti, and E. Louis, "Electrostatic edge modes of a hyperbolic dielectric wedge: Analytical solution," Phys. Rev. B **32**, 6045–6047 (1985).
[21]A. Eguiluz and A. A. Maradudin, "Electrostatic edge modes along a parabolic wedge," Phys. Rev. B **14**, 5526–5528 (1976).
[22]M. Debilly, "On the influence of loading on the velocity of guided acoustic waves propagating in linear elastic wedges," J. Acoust. Soc. Am. **100**, 659–662 (1996).
[23]V. V. Krylov, "On the velocities of localized vibration modes in immersed solid wedges," J. Acoust. Soc. Am. **103**, 767–770 (1998).
[24]C. Yang and I. Liu, "Optical visualization of acoustic wave propagating along the wedge tip," Proc. SPIE **8321**, 83211W (2011).
[25]D. Bogy, "Edge-bonded dissimilar orthogonal elastic wedges under normal and shear loading," J. Appl. Mech. **35**, 460–466 (1968).
[26]D. Bogy, "Two edge-bonded elastic wedges of different materials and wedge angles under surface tractions," J. Appl. Mech. **38**, 377–386 (1971).
[27]B. V. Budaev and D. B. Bogy, "Scattering of Rayleigh and Stoneley waves by two adhering elastic wedges," Wave Motion **33**, 321–337 (2001).
[28]E. Sokolova, A. Kovalev, A. Maznev, and A. Mayer, "Acoustic waves guided by the intersection of a surface and an interface of two elastic media," Wave Motion **49**, 388–393 (2012).
[29]R. Stoneley, "Elastic waves at the surface of separation of two solids," Proc. R. Soc. London **106**, 416–428 (1924).
[30]G. S. Murty, "Theoretical model for attenuation and dispersion of Stoneley waves at loosely bonded interface of elastic half spaces," Phys. Earth Planet. Int. **11**, 65–79 (1975).
[31]M. Schoenberg, "Elastic wave behavior across linear slip interfaces," J. Acoust. Soc. Am. **68**, 1516–1521 (1980).
[32]L. J. Pyrak-Nolte, L. Myer, and N. G. W. Cook, "Transmission of seismic waves across single natural fractures," J. Geophys. Res. **95**(B6), 8617–8638, doi:10.1029/JB095iB06p08617 (1990).
[33]S. Shao and L. J. Pyrak-Nolte, "Interface waves along fractures in anisotropic media," Geophys. **78**(4), T99–T112 (2013).
[34]D. L. Hopkins, "The implications of joint deformation in analyzing the properties and behavior of fractured rock masses, underground excavations and faults," Int. J. Rock Mech. Min. Sci. **37**, 175–202 (2000).
[35]C. Petrovitch, D. Nolte, and L. J. Pyrak-Nolte, "Scaling of fluid flow versus fracture stiffness," Geophys. Res. Lett. **40**, 2076–2080, doi:10.1002/grl.50479 (2013).
[36]R. Lubbe, J. Sothcott, M. H. Worthington and C. McCann, "Laboratory estimates of normal and shear fracture compliance," Geophys. Prospect. **56**, 239–247 (2008).
[37]C. Hobday and M. H. Worthington, "Field measurements of normal and shear fracture compliance," Geophys. Prospect. **60**, 488–499 (2012).
[38]D. Prikazchikov, "Rayleigh waves of arbitrary profile in anisotropic media," Mech. Res. Comm. **50**, 83–86 (2013).
[39]W. Ludwig and B. Lengeler, "Surface waves and rotational invariance in lattice theory," Solid State Commun. **2**, 83–86 (1964).
[40]Lord Rayleigh, "On waves propagated along the plane surface of an elastic solid," Proc. R. Soc. London A **17**, 4–11 (1885).
[41]L. J. Pyrak-Nolte and D. D. Nolte, "Wavelet analysis of velocity dispersion of elastic interface waves propagating along a fracture," Geophys. Res. Lett. **22**(11), 1329–1332, doi:10.1029/95GL01323 (1995).
[42]L. J. Pyrak-Nolte, J. Xu, and G. Haley, "Elastic interface waves propagating in a fracture," Phys. Rev. Lett. **68**(24), 3650–3653 (1992).
[43]P. Vinh and R. W. Ogden, "On formulas for the Rayleigh wave speed," Wave Motion **39**, 191–197 (2004).
[44]P. Chadwick, "The existence of pure surface modes in elastic materials with orthorhombic symmetry," J. Sound Vib. **47**(1), 39–52 (1976).